Delamination Failure Mechanisms in Microlayers of Polycarbonate and Poly(styrene-*co*-acrylonitrile)

T. EBELING, A. HILTNER, E. BAER

Department of Macromolecular Science and Center for Applied Polymer Research, Case Western Reserve University, Cleveland, Ohio 44106, USA

Received 25 September 1997; accepted 28 October 1997

ABSTRACT: The peel strength and delamination failure mode of coextruded microlayer sheets consisting of alternating layers of polycarbonate (PC) and poly(styrene-*co*-acrylonitrile) (SAN) were studied with the T-peel test. Four delamination modes were observed: two modes where the crack propagated along the PC–SAN interface and two other modes where the crack propagated through crazes in the SAN. The SAN layer thickness determined whether crack propagation was interfacial or through crazes. Crazing and crack propagation through crazes were observed only if the SAN layer was thicker than 1.5 μm. As the thickness of the SAN layer increased, the amount of crazing in front of the crack tip and the amount of craze fracture gradually increased; the peel strength increased accordingly. If the SAN layers were thinner than 1.5 μm and the PC layers were relatively thick, the crack propagated along a single interface. The peel strength for this delamination mode was the lowest and equal to about 90 J/m^2, independent of layer thicknesses. This delamination mode came closest to providing a "real" measure of the adhesive toughness of PC to SAN. With both interfacial and craze delamination, the crack could move from layer to layer if the PC was thin enough. Tearing of the relatively thin PC layers increased the peel strength of the multiple-layer delamination modes. © 1998 John Wiley & Sons, Inc. J Appl Polym Sci 68: 793–805, 1998

Key words: polycarbonate; poly(styrene-*co*-acrylonitrile); microlayers; peel strength

INTRODUCTION

The development of interfacial strength between immiscible polymers in the rubbery or melt state is fundamental to polymer blend technology. Good adhesion requires polymer chains to diffuse across the interface far enough to become entangled. This can only happen if the polymers are close to miscibility. Polymers that are not miscible but are close enough to develop good interfacial strength can be described as compatible. Polycarbonate (PC) and poly(styrene-*co*-acrylonitrile) (SAN) fall into this category. An important consequence is that good properties can be achieved without adding a compatibilizer to blends of PC with SAN[1–3] and blends of PC with acrylonitrile–butadiene–styrene (ABS) which has a SAN matrix.[4–6] The commercial importance of PC–ABS blends and the possibility for varying the PC–SAN interaction by changing the acrylonitrile (AN) content provided the impetus for previous studies of PC–SAN adhesion.[7–11]

Polycarbonate and SAN can be coextruded as a continuous microlayered sheet with hundreds of alternating layers. Increased toughness and impact resistance when the thickness of the layers is reduced from the macroscale (tens of microns) to the microscale (several microns) is attributed to fundamental changes in the deformation behavior. The cooperative microdeformation mecha-

Correspondence to: A. Hiltner.
Contract grant sponsor: National Science Foundation; contract grant number: DMR 9400475.

Journal of Applied Polymer Science, Vol. 68, 793–805 (1998)
 CCC 0021-8995/98/050793-13

nisms responsible for increased toughness are only possible because adhesion between the components is good enough to ensure stress transfer under conditions of high deformation.[12–16] Similarly, ductile deformation of micron-size ABS and SAN particles in blends with PC contributes to the high energy-absorbing capability of these blends.[17] Synergistic interactions of crazes and shearbands require the interface to withstand large strains without failing. A similar requirement applies to polymer blends where high strains in one or both components provide the energy absorption for enhanced toughness. The microlayers provide a model system for understanding these interfacial strength requirements.

It has been recognized for some time that normal test methods can give values for the interfacial toughness of immiscible polymers that are unexpectedly high.[18–20] Often, the high values are caused by crazing in the polymer with the lower craze resistance. It appears likely that crazing was a factor in previous measurements of PC–SAN interfacial strength and the reported values may therefore be too high. Interfacial strength of microlayered polymers can be measured by the straightforward peel method. Because the individual layers are relatively thin, comparable to the thickness of a conventional adhesive layer, it is necessary to consider possible effects of layer thickness. Although thickness of the adhesive layer does not usually affect the measured value of the adhesive fracture energy for relatively brittle adhesives, for tougher adhesives that form a large damage zone and may fracture cohesively, this parameter can significantly affect the measured value.[21–24] The toughness generally increases with the thickness of the adhesive layer as the restriction on the development of the plastic zone is reduced, and it reaches a maximum when the adhesive layer thickness and the plastic zone diameter are approximately equal. Sometimes, the maximum toughness also coincides with a transition in the mode of crack propagation.

In this study, interfacial strength was measured by peeling PC/SAN microlayers. To evaluate the contribution of crazing to delamination, the effects of PC and SAN layer thicknesses on the delamination strength were examined using SAN with 25% AN. The delamination mode was characterized by microscopic examination and infrared analysis. Based on these results, conditions for measuring interfacial strength were established. The possible influence of oligomers in the SAN component on interfacial strength was also taken into consideration.

Table I Layer Thickness and Delamination Toughness of PC/SAN Microlayers

Layer Thickness (PC/SAN) (μm/μm)	Delamination Mode	Delamination Toughness (J/m^2)
15.0/0.5	Single interface	95 ± 3
14.0/0.7	Single interface	90 ± 10
13.5/1.4	Single interface	130 ± 3
9.1/0.2	Single interface	95 ± 4
4.5/0.5, low oligomers	Single interface	94 ± 6
5.0/0.5	Single interface	98 ± 6
4.2/0.5	Single interface	88 ± 8
2.5/0.5	Single interface	92 ± 6
2.2/0.9	Single interface	94 ± 6
1.8/1.0	Single interface	135 ± 8
1.6/0.5	Multiple interface	180 ± 20
1.2/0.2	Multiple interface	236 ± 20
1.1/0.5	Multiple interface	295 ± 10
1.1/1.4	Multiple interface	420 ± 40
0.9/1.4	Multiple interface	310 ± 55
0.8/0.7	Multiple interface	290 ± 30
0.5/1.0	Multiple interface	256 ± 30
8.1/1.6	Single-layer craze	135 ± 3
9.2/2.8	Single-layer craze	165 ± 15
8.2/4.2	Single-layer craze	180 ± 10
6.8/5.6	Single-layer craze	220 ± 20
5.0/7.5	Single-layer craze	300 ± 40
34.0/18.0	Single-layer craze	320 ± 115
28.0/24.0	Single-layer craze	440 ± 40
20.0/30.0	Single-layer craze	400 ± 80
14.0/37.0	Single-layer craze	650 ± 110
3.1/8.7	Multiple-layer craze	550 ± 140
2.8/17.0	Multiple-layer craze	480 ± 80

EXPERIMENTAL

Coextruded microlayer sheets were either supplied by The Dow Chemical Co.[25] or coextruded using the layer multiplying process described previously.[26] Sheets 1–2 mm in thickness consisted of alternating layers of PC and SAN. The number of layers and the extruder feed ratios were varied to produce microlayers with different compositions and layer thicknesses. The number of layers varied from 49 to 1857, and the feed ratio varied from PC/SAN 26/74 to 90/10 (wt/wt). The samples are identified by the layer thicknesses in Table I. The average layer thicknesses were calcu-

lated from the measured bulk thicknesses, the total number of layers, and the feed ratio.

The PC was Merlon M-40 (Mobay) with a molecular weight of 28,000–30,000 reported by the manufacturer. The SAN was Tyril 1000B (previously Tyril 867B; Dow) with a molecular weight of 193,000 and a polydispersity of 1.9 as determined by GPC relative to polystyrene standards with the appropriate correction.[27] The 25% AN content reported by the manufacturer was confirmed by FTIR.[28]

Oligomers were removed from SAN by dissolving the as-received SAN in acetone at a concentration of 3 g/dL, precipitating in isopropanol, filtering, and drying in a vacuum at 90°C for 24 h. The oligomer content was estimated from the glass transition temperature using the Fox equation with −56.0°C as the T_g of the oligomer and 116.0°C as the T_g of oligomer-free SAN with 25% AN.[29] The glass transition temperature was obtained by differential scanning calorimetry using a Rheometrics DSC Plus with a dry nitrogen purge and a heating rate of 20°C/min. The temperature was calibrated with indium and tin, and the glass transition temperature was taken from the second heating thermogram. The as-received SAN had a T_g of 111.8°C, indicating an oligomer content of about 1.4%, consistent with previous findings on commercial SAN resins.[29,30] The reprecipitated SAN had a T_g of 115.3°C, indicating an oligomer content of about 0.2%. In microlayers, the T_g of as-received SAN increased from 111.8 to 115.0°C (0.2% oligomer) and the T_g of the reprecipitated SAN shifted slightly from 115.3 to 116.0°C (<0.1% oligomer). Similar shifts in the T_g of SAN in PC/SAN blends were attributed to the diffusion of SAN oligomers into the PC.[29,30]

Delamination was carried out with the T-peel test (ASTM D 1876). Specimens 15–25 mm wide were notched by pushing a fresh razor blade into the midplane of the sheet. The notch was examined with an optical microscope to ensure that the crack started along a single layer. Specimens were loaded at a rate of 2.0 mm/min.

Some tests were interrupted and the crack tip region was sectioned perpendicular to the plane of the crack with a low-speed diamond saw (Isomet, Buehler Ltd.). The sections were polished on a metallurgical wheel with wet sandpaper and alumina oxide aqueous suspensions. The sections were photographed in a transmission optical microscope. Sections of the fracture surfaces were coated with 90 Å of gold for examination in a JEOL JSM 840A scanning electron microscope. Uncoated sections of the fracture surface were characterized with a Nicolet 800 FTIR spectrometer in the ATR mode with a germanium 60/60 crystal to determine the composition.

RESULTS AND DISCUSSION

Peel Strength

Beam arm curvature in the T-peel test was compared to Kendall's elastic prediction[31] to determine if the beam arms deformed elastically. The calculation assumed that the microlayer modulus followed the rule of mixtures. Figure 1 shows an example where the curvature during crack propagation matched the elastic prediction. Plastic deformation of the beam arms would have been indicated by a curvature much sharper than that predicted by elastica. The curvature of all the PC/SAN microlayers except two matched elastica; the two exceptions were PC/SAN (3.1/8.7 μm) and (2.6/16.4 μm). The beam arms were also visually examined for plastic deformation as indicated by the failure of the beam arms to return to their original positions upon removal of the load. Only the beam arms of the two samples that did not match elastica did not return to their original positions. In most cases, the beams behaved elastically and negligible energy was spent on plastic deformation of the beam arms. The measurement of resistance to crack propagation, however, may

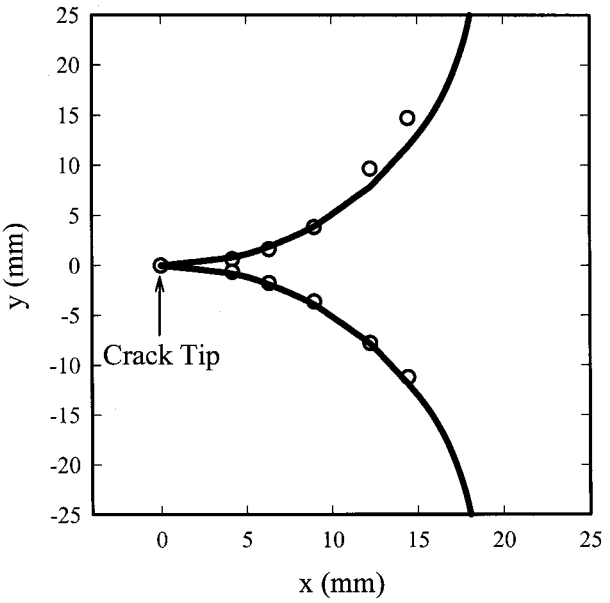

Figure 1 Comparison of measured beam arm profile of PC/SAN (34/18 μm) (symbols) with elastic prediction (line).

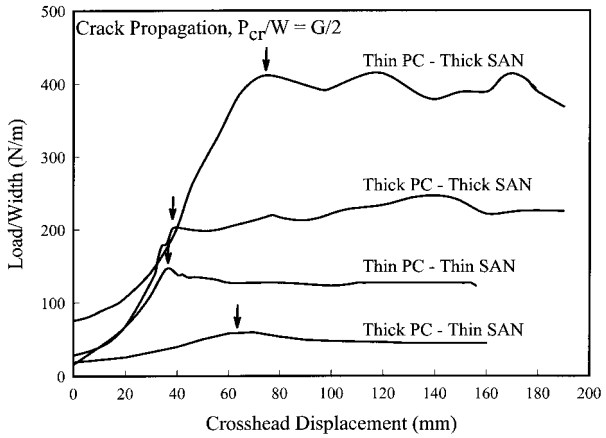

Figure 2 Normalized peel curves of four typical samples: thick PC–thin SAN (2.5/0.5 μm), thin PC–thin SAN (0.5/1.0 μm), thick PC–thick SAN (34/18 μm), and thin PC–thick SAN (3.1/8.7 μm).

include contributions from the damage zone in front of the crack tip.

The load-displacement curves of the four PC/SAN microlayers shown in Figure 2 cover the ranges of PC and SAN layer thicknesses tested. The load initially increased while the crack remained stationary and the beam arms bent into the T-peel configuration. The crack then propagated in a stable manner at a relatively constant load, P_{cr}, from which the delamination toughness, $G = 2P_{cr}/W$, was obtained for a specimen of width W. Changing only the layer thicknesses increased the peel strength by almost an order of magnitude. Two trends were observed: Peel strength was lower with thin SAN layers than with thick SAN layers, and peel strength was higher with thin PC layers than with thick PC layers. Failure analysis revealed that layer thicknesses controlled the peel strength through the mode of crack propagation.

Single-interface Delamination with Thin SAN Layers and Thick PC Layers

The sample with the lowest peel strength in Figure 2 had thin SAN layers (0.5 μm) and thick PC layers (2.5 μm). Optical microscopy of the crack tip showed that the crack propagated primarily along a single interface, although debonding was occasionally observed ahead of the crack tip at both interfaces of the SAN layer. The composition of the delaminated surfaces was identified by ATR–FTIR. One surface exhibited strong SAN peaks at 701, 760, 1451, 1492, and 2235 cm^{-1} and very weak PC peaks at 1163, 1191, 1233, 1505, and 1776 cm^{-1} [Fig. 3(a)]. Conversely, the matching surface showed strong PC peaks and barely detectable SAN peaks [Fig. 3(b)]. The presence of primarily SAN on one fracture surface and primarily PC on the other fracture surface confirmed the interfacial crack propagation.

Although visually featureless and transparent, the fracture surfaces contained microscale features. An SEM micrograph of an SAN surface [Fig. 3(c)] shows "wrinkles" perpendicular to the crack growth direction. The wrinkles were a manifestation of the SAN layer debonding and pulling away from the underlying PC layer. The wrinkles occasionally had holes through which the underlying PC layer could be seen. The holes in the SAN layer matched "chunks" of material dispersed about the otherwise smooth PC surface [Fig. 3(d)]. These chunks were pieces of SAN that remained adhered to the PC layer. Rather than debonding at these points, the SAN fractured and chunks were pulled out.

A schematic representation of single-interface delamination is shown in Figure 4. As the crack propagated along a single interface, it was sporadically preceded by debonding at either interface of the SAN layer [Fig. 4(a)]. The debonding probably resulted from local variations in adhesive strength or from small scale yielding of SAN at the crack tip. The SAN layer pulled out where it debonded from the underlying PC layer and a wrinkle remained after crack propagation released the SAN layer [Fig. 4(b)]. In spots where interfacial adhesion in the crack plane was particularly good, the SAN layer was not completely released; instead, a chunk of SAN was pulled out [Fig. 4(c)]. This left a hole in the wrinkle on the SAN layer and a chunk of SAN on the PC layer.

Single-interface delamination occurred if the PC layer thickness was 1.7 μm or more and the SAN layer thickness was 1.5 μm or less. If the SAN layer thickness was less than 1.5 μm, it broke more easily and the density and size of SAN chunks on the PC fracture surface increased. However, this had no measurable effect on the delamination toughness, which, for single-interface delamination, was independent of both PC and SAN layer thicknesses and equal to 90 ± 8 J/m^2 (Table I). Removing the oligomer from SAN did not affect the single-interface delamination. Microlayers of reprecipitated SAN with 0.5 μm SAN layers and 4.5 μm PC layers failed by single-interface delamination with a measured delamination toughness of 94 ± 6 J/m^2. Previous reports that oligomers affect the PC/SAN adhesive (delamination) toughness are probably misleading

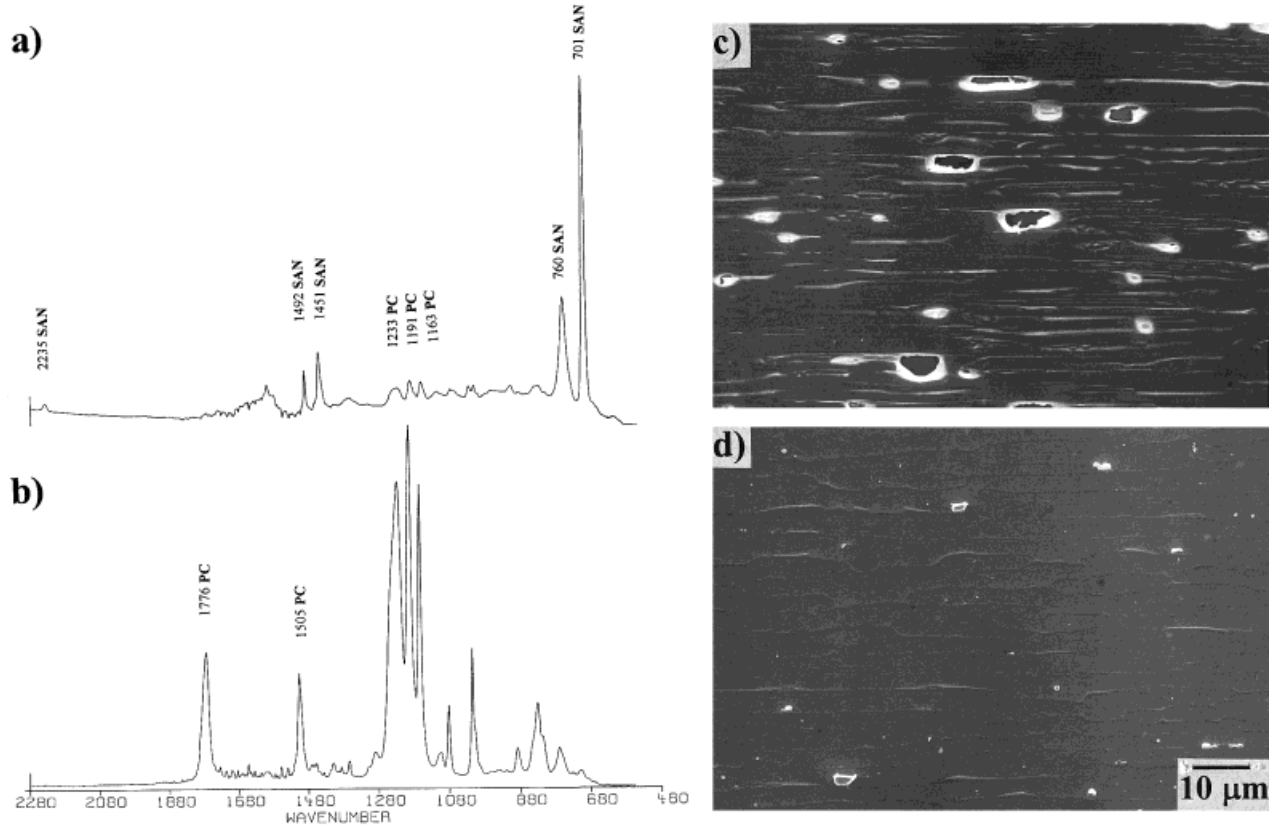

Figure 3 FTIR–ATR spectra and SEM of opposite peel fracture surfaces from PC/SAN (2.5/0.5 μm).

because craze damage accompanied the delamination.[17] Interfacial delamination was essentially a brittle fracture mode. The constant delamination toughness, independent of layer thickness, was consistent with a mechanism controlled by the resistance of the interface to flaw formation.

Multiple-interface Delamination with Thin SAN Layers and Thin PC Layers

The peel strength of microlayers with thin SAN layers (1.5 μm or less) increased when the PC layer thickness was less than 1.7 μm. This was due to a change in the delamination mode from single- to multiple-interface delamination. Examination of the crack tip of PC/SAN (0.45/1.0 μm) revealed debonding at several SAN layers ahead of the crack tip. The crack subsequently propagated along several interfaces and tore through both PC and SAN layers as it moved from interface to interface.

The FTIR spectra indicated that both surfaces had the same composition with approximately equal amounts of PC and SAN. In addition, the matching fracture surfaces exhibited the identical texture in the SEM. Although the PC and SAN layers could not be differentiated in the SEM micrographs of the fracture surfaces, fragments of many layers were distinguishable by the torn edges (Fig. 5). Four different layers are identified in Figure 5, numbered from 1 (bottommost) to 4 (topmost). Although the jagged boundaries gave the surface a slight visual haziness, the smoothness of the layers indicated that the crack propagated by interfacial delamination.

A schematic representation of multiple-interface delamination is shown in Figure 6. Because the layers were thin, neighboring interfaces exhibited areas of debonding ahead of the crack tip [Fig. 6(a)]. Stress redistribution as the debonded areas enlarged, coupled with the very thin layers which were easily torn, enabled the crack to move from one interface to another [Fig. 6(b)]. Consequently, crack propagation included a large number of layer-to-layer jumps [Fig. 6(c)].

The relationship between delamination toughness and PC layer thickness in microlayers with SAN layers thinner than 1.5 μm is illustrated in Figure 7. Microlayers with PC layers thicker than 1.7 μm exhibited single-interface delamination

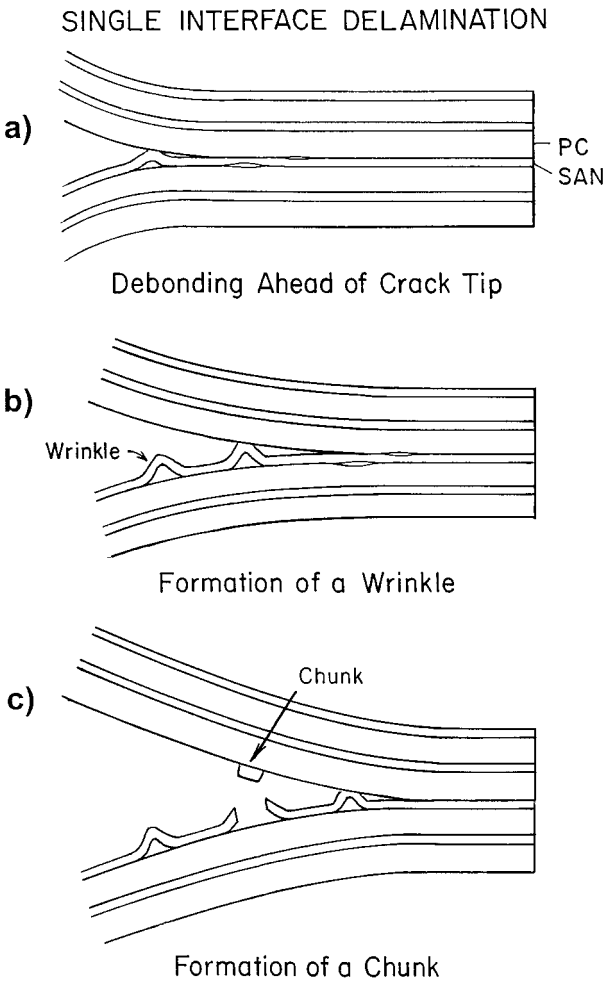

Figure 4 Schematic representation of single-interface delamination.

(open circles); those with PC layers thinner than 1.7 μm exhibited multiple-interface delamination (filled symbols). The delamination toughness for multiple-interface delamination was higher than

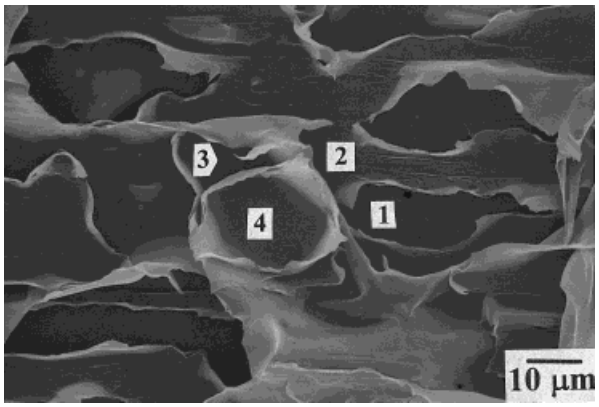

Figure 5 SEM of peel fracture surface from PC/SAN (0.5/1.0 μm). Numbers indicate different layers along which the crack propagated.

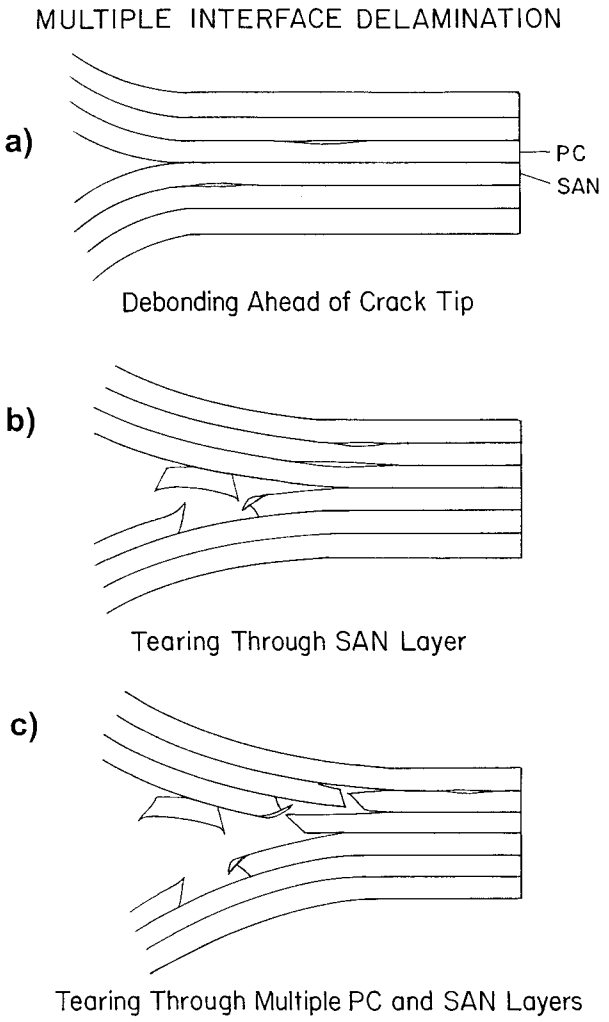

Figure 6 Schematic representation of multiple-interface delamination.

that for single-interface delamination due to the additional force required to tear the layers. Unlike single-interface delamination, multiple-interface delamination toughness increased with decreasing PC layer thickness as more of the thinner layers were torn.

Thick PC layers confined debonding and crack propagation to the interfaces of a single SAN layer. As the PC layers became thinner, the stress at the interfaces of neighboring SAN layers increased until it was high enough to cause debonding. Furthermore, as the PC thickness decreased, the PC layers tore more easily. This enabled the crack to move from one interface to another and, accordingly, the energy absorbed tearing the thin PC and SAN layers increased the peel strength. For the PC/SAN system, the stress field associated with an interfacial crack produced significant deformation and damage at neighboring in-

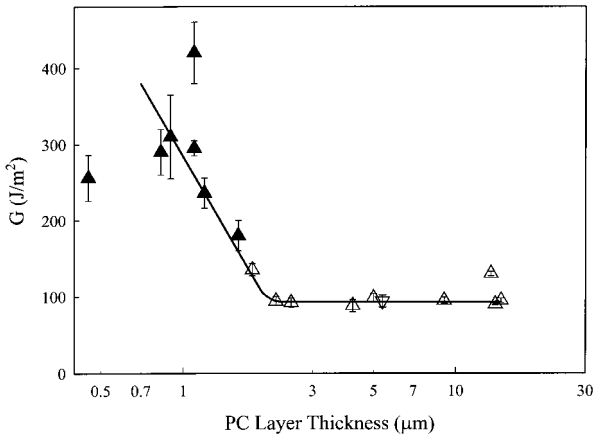

Figure 7 Peel toughness as a function of PC layer thickness for samples with SAN layers thinner than 1.5 μm. Filled triangles represent multiple-interface delamination, open triangles represent single-interface delamination, and the downward triangle represents single-interface delamination of the sample with reprecipitated SAN.

terfaces when the PC layer thickness was at or below a critical value of 1.7 μm. Possibly, the 1.7-μm PC thickness is a more general condition for interactive deformation in PC/SAN microlayers. In another study, a transition from random to cooperative crazing in SAN layers occurred at about the same PC layer thickness.[32]

Single-layer Craze Delamination with Thick SAN Layers and Thick PC Layers

Crazing was observed in SAN layers thicker than 1.5 μm. The micrograph of PC/SAN (8.2/4.2 μm) in Figure 8(a) shows four or five crazes ahead of the crack tip. The crazes were confined to a single SAN layer; they initiated at one of the interfaces and grew through the SAN layer to the other interface at an angle of about 55° to the horizontal. Residual stresses created by the differences in T_g and thermal expansion coefficient of SAN and PC probably facilitated crazing ahead of the crack tip.[33] Shear stresses, produced by the modulus mismatch between PC and SAN, changed the principal stress directions[34,35] and caused the crazes to grow at an angle.[36,37] The micrograph also shows that the crack propagated alternately through crazes and along either interface of the crazing SAN layer.

Fractured specimens were visually opaque due to light scattering from the fracture surface. Under magnification, the texture of the fracture surface confirmed that the crack propagated alternately through crazes and along both interfaces of the crazing SAN layer. The left side of the SEM in Figure 8(b) shows a smooth surface littered with chunks of material, typical of the PC surface with chunks of SAN after interfacial delamination. The porous texture in the middle of the figure is typical of SAN craze fracture. The features are produced by the fracture of craze fibrils when the crack propagated through the center of the craze. The smooth region with wrinkles on the right side of the figure is characteristic of the SAN surface after interfacial fracture. As the crack moved from left to right in Figure 8(b), it started at one interface, then followed a craze through the SAN layer to the other interface. Crazing and crack propagation through crazes increased the peel toughness to 180 J/m^2 for this microlayer sample.

The FTIR spectra of matching fracture surfaces from single-layer craze delamination were virtually the same with relatively weak PC peaks accompanied by stronger SAN peaks (Fig. 9). The spectra confirmed the presence of more SAN than PC on the fracture surfaces as expected for a crack that alternately propagated through crazes,

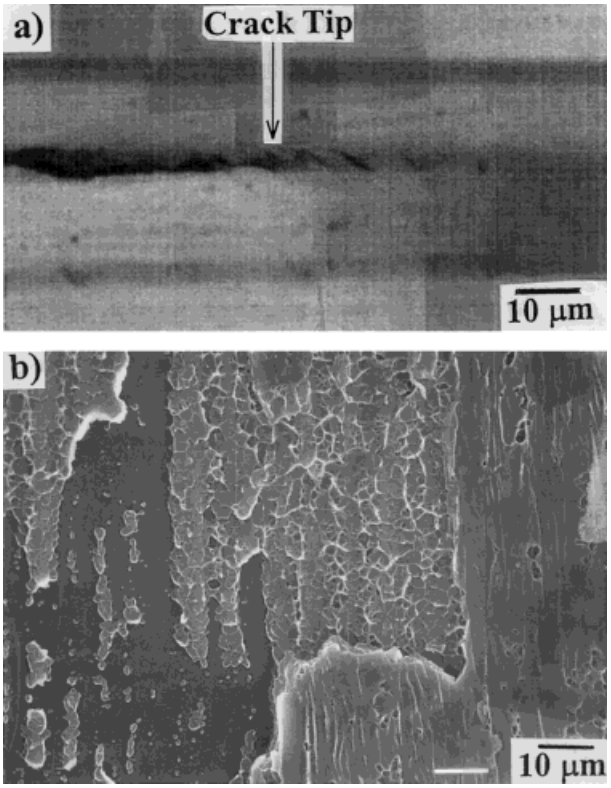

Figure 8 (a) Optical micrograph of PC/SAN (8.2/4.2 μm) crack tip; (b) SEM of peel fracture surface from PC/SAN (8.2/4.2 μm). The crack propagated from left to right.

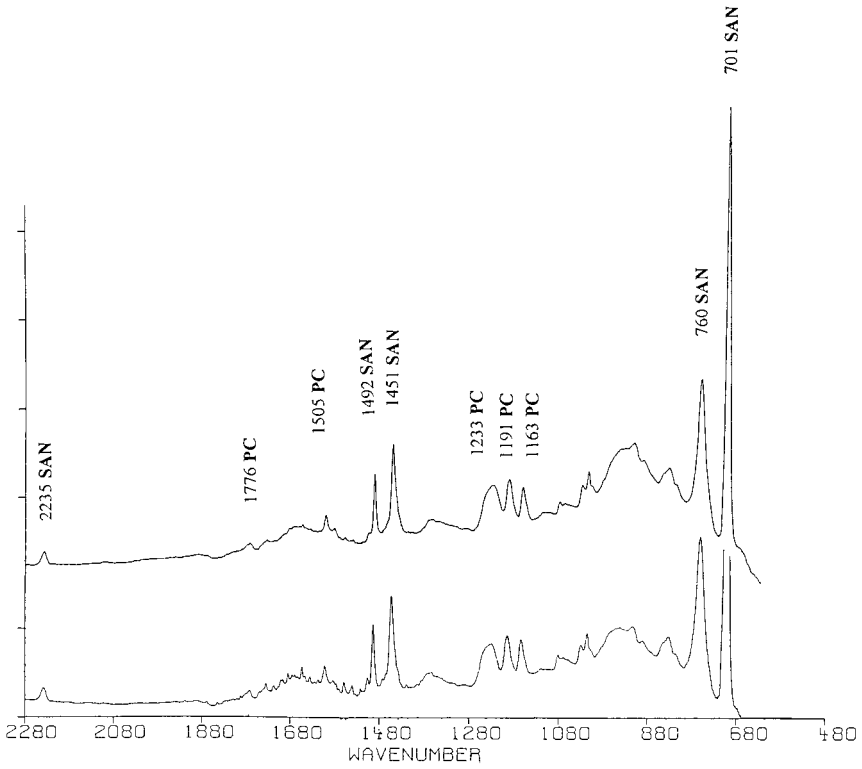

Figure 9 FTIR–ATR spectra from matching surfaces of craze delamination.

which left SAN on both surfaces, and along either interface, which left SAN on one surface and PC on the matching surface.

The angle of the crazes in front of the crack tip increased with increasing SAN layer thickness from about 30° in 1.6-μm-thick SAN layers to 90° in SAN layers that were thicker than 10 μm. The changing craze angle reflected the increase in shear stress with layer thickness.[38,39] As the crazes approached a vertical orientation, they provided a more difficult pathway for the propagating crack, and a second population of crazes started to appear ahead of the crack tip. These crazes were only observed with thicker SAN layers. They originated from the crack tip and curved over toward one of the interfaces. As the optical micrograph of PC/SAN (34/18 μm) in Figure 10 illustrates, these crazes were confined to about half of the SAN layer.

Figure 11 is a schematic representation of single-layer craze delamination with SAN layers thicker than 10 μm. The fracture process began with the formation of vertical crazes, followed by a second population of horizontal crazes that grew from the crack tip. The crack propagated through one of the horizontal crazes and bent over toward the interface following the path of the craze [Fig. 11(a)]. Often, the crack moved to a neighboring craze before reaching the interface [Fig. 11(b)]. The crack moved from one craze to another either by following impinging crazes or by jumping from one craze to another through a vertical craze. Occasionally, the crack followed a craze all the way to the interface and then propagated along the interface [Fig. 11(c)], until it followed a vertical craze to jump back to the horizontal crazes. The FTIR spectrum of the fracture surface from the upper beam arm in Figure 10 exhibited only strong SAN peaks and that of the matching surface exhibited both PC and SAN peaks as expected if the crack alternately propagated through crazes in the SAN layer and along a single PC-SAN interface.

The micrographs in Figure 12 show the fracture surfaces of the specimen in Figure 10. Figure 12(a) is from the upper beam arm that had only SAN peaks in the FTIR and Figure 12(b) is the matching area from the lower beam arm with both PC and SAN peaks in the FTIR. The crack direction was left to right. Both contain a large area of craze fracture in the center. The bright lines in the craze regions that are perpendicular to the crack direction indicate steps in the topology where the crack jumped along a vertical craze.

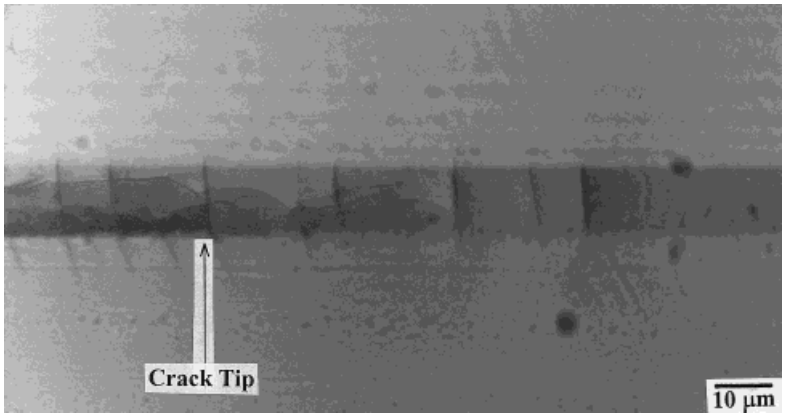

Figure 10 Optical micrograph of PC/SAN (34/18 μm) crack tip.

Tilting the SEM stage revealed these steps to be about 10 μm or approximately half the thickness of the SAN layer. After each step, the crazed surface gradually sloped toward the interface as it would if it were following a craze that curved over toward the interface. Near the edges of the micrographs are areas of smoother texture that are not identical on the matching surfaces. A boundary between crazed and smooth texture is shown at higher magnification in Figure 12(c, d). The craze texture to the left is the same on both surfaces and characteristic of fibril fracture. The textures on the smooth regions are typical of interfacial delamination. Wrinkles and holes are seen where the SAN layer is exposed on the right side of Figure 12(c), and smooth areas littered with chunks of material are seen where the matching PC layer is exposed on the right side of Figure 12(d).

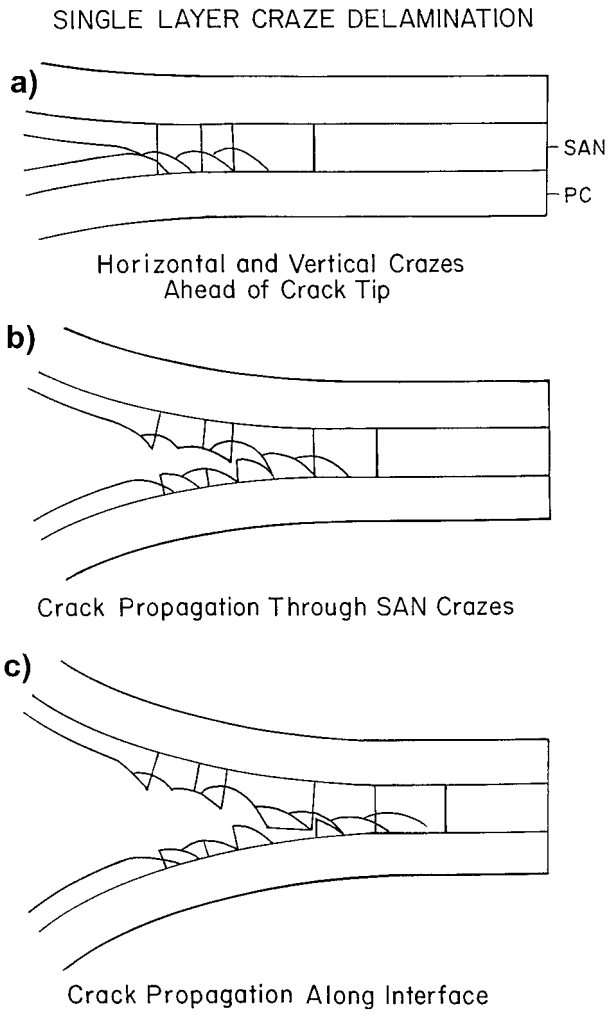

Figure 11 Schematic representation of single-layer craze delamination.

The delamination toughness of microlayers with thick SAN and thick PC layers is plotted as a function of SAN layer thickness in Figure 13. The toughness initially increased rapidly as the SAN layer thickness increased from 1.5 to 8.5 μm. Rapid increases in the number of crazes and the amount of craze fracture relative to interfacial fracture accounted for this effect. After the SAN layer thickness reached about 10 μm, the toughness increased at a slower rate. The slope change in Figure 13 occurred when the crazing habit of the SAN layer changed from only angled crazes to vertical crazes together with horizontal crazes. The decreased slope at higher SAN layer thicknesses reflected smaller rates of increase in craze density and the amount of craze fracture relative to interfacial fracture.

Multiple-layer Craze Delamination with Thick SAN Layers and Thin PC Layers

Samples with SAN layers thicker than 1.5 μm and relatively thin PC layers had the highest peel strength. During peel tests of these samples, the

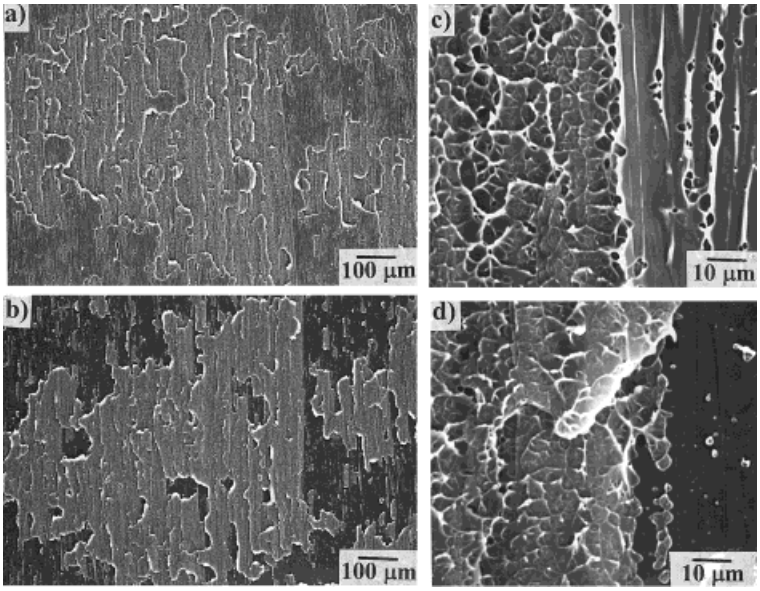

Figure 12 Low (a, b) and high (c, d) magnification SEM of matching peel fracture surfaces from PC/SAN (34/18 μm). The crack propagated from left to right.

beam arms did not conform to the elastic beam curvature, and they exhibited permanent deformation after the load was removed. A micrograph of PC/SAN (4.4/9.3 μm) in Figure 14 shows that crazing in front of the crack tip extended to at least nine SAN layers. Alignment of crazes in neighboring SAN layers indicated cooperative crazing similar to that described in tensile deformation.[10] Other micrographs showed that the crack often jumped from crazes in one SAN layer to crazes in the next, tearing the intervening PC layer. The fracture surfaces were almost completely covered with craze features. Sharp steps indicated where the crack jumped from one SAN layer to another. The FTIR spectra of both fracture surfaces exhibited strong SAN peaks and only very small PC peaks, consistent with crack propagation almost exclusively through the SAN layers and rarely if ever along an interface.

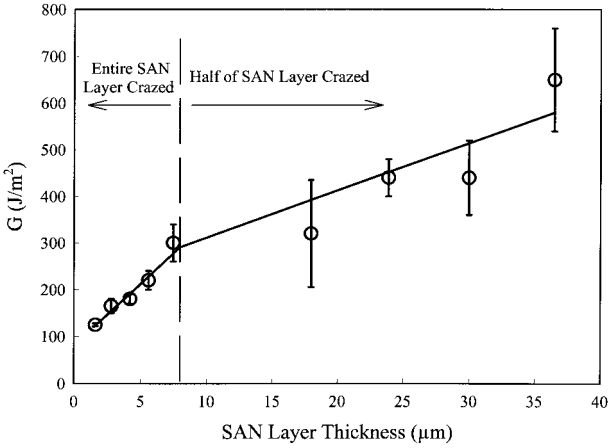

Figure 13 Peel strength as a function of SAN layer thickness for samples which failed by single-layer craze delamination.

The multiple-layer craze delamination mode is illustrated schematically in Figure 15. Crazes grew out of the crack tip in the SAN layer, curved over, and arrested at the interface [Fig. 15(a)]. Because of the close proximity of the next SAN layer, the stress concentration at the craze tip was sufficient to initiate crazing in the neighboring SAN layer [Fig. 15(b)]. Occasionally, crazes in a neighboring SAN layer coalesced to form a microcrack. Microcracks provided a route for the primary delamination crack to move from one SAN layer, through the PC layer, into the neighboring SAN layer [Fig. 15(c)].

Map of Delamination Modes

Figure 16 summarizes the relationship of the four delamination modes to PC and SAN layer thicknesses. Open and filled circles indicate the two crazing modes, and open and filled triangles indicate the two interfacial modes. The SAN layer thickness determined whether the delamination mode was crazing or interfacial. If the SAN layer was thinner than 1.5 μm, crazing was suppressed and interfacial delamination occurred. In a previous study of PS adhesion to PMMA, it was also

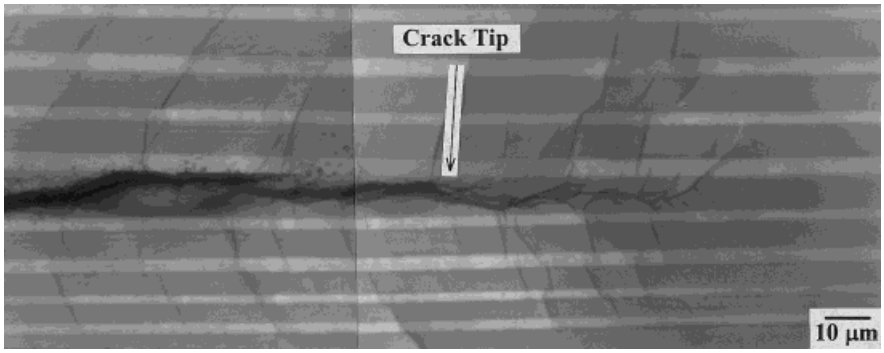

Figure 14 Optical micrograph of PC/SAN (3.1/8.7 μm) crack tip.

observed that the PS had to be thicker than 1.5 μm for a cleavage crack to propagate through crazes in the PS; otherwise, the PS did not craze.[18] A critical thickness of 1.5 μm for crazing may be a manifestation of the stress distribution at a delamination crack tip in microlayers of SAN with a dissimilar material. Alternatively, it may be an inherent characteristic of styrenic polymers.

In both interfacial and craze delamination modes, it was possible for the crack to propagate along either a single layer or through multiple layers. The multiple-layer delamination modes required thin PC layers so that the stresses at adjacent interfaces would be high enough to initiate secondary delamination cracks and also so that the intervening PC layer could tear as the fracture plane moved from one layer to another. Experimentally, the critical PC layer thickness for multiple-layer interface delamination was 1.7 μm. The condition was independent of SAN layer thickness in part because the SAN layers were always thin when the delamination mode was interfacial and any effect that would be revealed by thick SAN layers could not be evaluated. Also, SAN layers were not as tough as PC layers as seen in the

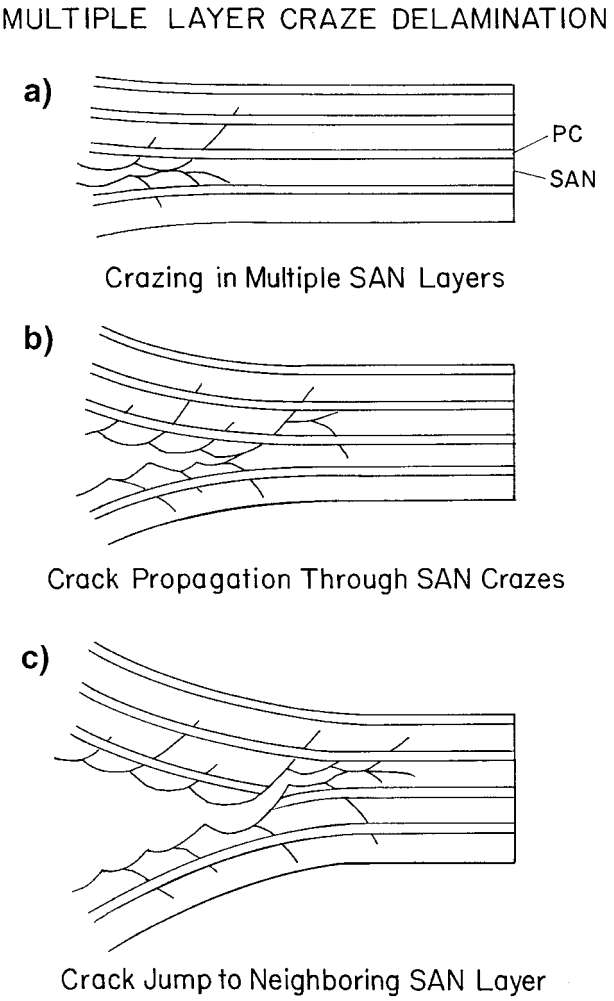

Figure 15 Schematic representation of multiple-layer craze delamination.

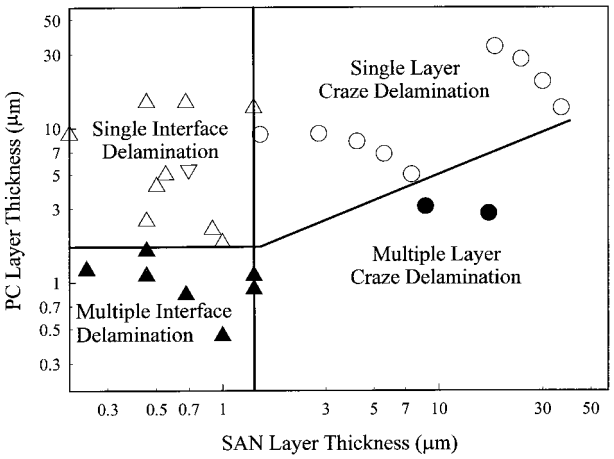

Figure 16 Delamination mechanism as a function of PC and SAN layer thickness. Symbol position represents layer thicknesses of samples; symbol type represents delamination mode.

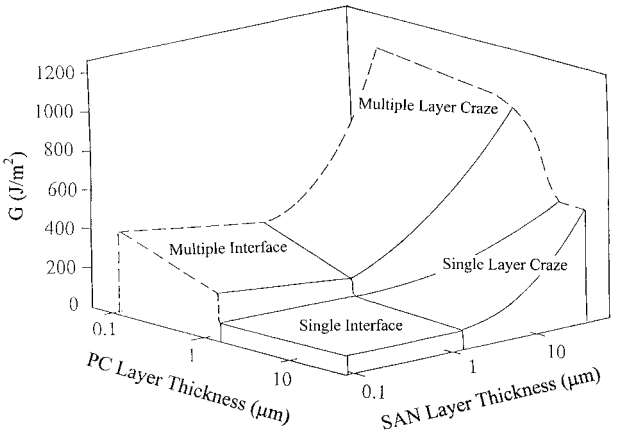

Figure 17 Three-dimensional plot of peel toughness as a function of PC and SAN layer thicknesses.

propensity for SAN chunks to break off during delamination without noticeably affecting the interfacial delamination toughness. Therefore, it seems reasonable that the condition for the crack to move from one interface to another should be determined only by the energy required to tear the intervening PC layer, and, hence, by the PC layer thickness.

The condition for multiple-layer craze delamination appeared to depend on both SAN and PC layer thicknesses. Because single-layer delamination toughness increased with increasing SAN layer thickness, the thickness of the PC layers that could tear and produce multiple-layer delamination also increased. Accordingly, the PC layers of the two microlayer compositions that exhibited multiple-layer craze delamination were thicker than 1.7 μm. The relationship between PC and SAN layer thicknesses at the transition from single-layer to multiple-layer craze delamination is represented as linear in Figure 16, although it may be more complex.

A three-dimensional plot in Figure 17 combines the delamination toughness with the four delamination modes. The toughness for multiple-layer delamination was always higher than for single-layer delamination due to tearing of the PC layers. Cooperative crazing in neighboring SAN layers also contributed to the multiple-layer craze delamination strength. Thicker PC layers confined delamination to a single SAN layer and the toughness was lower than when the crack could move from one layer to another. The toughness was lowest for single interface delamination, 90 $\pm$ 8 J/m^2. Because there was no crazing, and the measured toughness was independent of both PC and SAN layer thicknesses, this delamination mode came closest to providing a "real" measure of the adhesive toughness of PC to SAN. The single-layer delamination toughness increased when the SAN layers were able to craze. The number of crazes and the amount of craze fracture increased with the SAN layer thickness, and the delamination toughness correspondingly increased as much as five times.

The authors wish to thank Mr. Anand Shah for his assistance with the peel experiments and Dr. A. Hsieh of The Army Research Laboratory, Aberdeen, MD, Dr. J. Im of The Dow Chemical Co., Midland, MI, and Dr. C. Sellitti for their numerous technical contributions. The generous financial support of the National Science Foundation (DMR 9705696) is gratefully acknowledged.

REFERENCES

1. R. E. Skochdopole, C. R. Finch, and J. Marshall, *Polym. Eng. Sci.,* **27,** 627 (1987).
2. D. Quintens, G. Groeninckx, M. Guest, and L. Aerts, *Polym. Eng. Sci.,* **30,** 1474 (1990).
3. D. Quintens, G. Groeninckx, M. Guest, and L. Aerts, *Polym. Eng. Sci.,* **31,** 1215 (1991).
4. M.-P. Lee, A. Hiltner, and E. Baer, *Polym. Eng. Sci.,* **32,** 909 (1992).
5. M.-P. Lee, A. Hiltner, and E. Baer, *Polym. Eng. Sci.,* **32,** 909 (1992).
6. M. Ishikawa, *Polymer,* **36,** 2203 (1995).
7. J. D. Keitz, J. W. Barlow, and D. R. Paul, *J. Appl. Polym. Sci.,* **29,** 3131 (1984).
8. V. Janarthanan, R. S. Stein, and P. D. Garrett, *J. Polym. Sci. B Polym. Phys.,* **31,** 1995 (1993).
9. J. L. Willett and R. P. Wool, *Macromolecules,* **26,** 5336 (1993).
10. T. A. Callaghan, K. Takakuwa, D. R. Paul, and A. R. Padwa, *Polymer,* **34,** 3796 (1993).
11. V. H. Watkins and S. Y. Hobbs, *Polymer,* **34,** 3955 (1993).
12. M. Ma, K. Vijayan, J. Im, A. Hiltner, and E. Baer, *J. Mater. Sci.,* **25,** 2039 (1990).
13. J. Im, E. Baer, and A. Hiltner, in *High Performance Polymers,* E. Baer and A. Moet, Eds., Hanser, New York 1991, pp. 175–198.
14. E. Shin, A. Hiltner, and E. Baer, *J. Appl. Polym. Sci.,* **47,** 269 (1993).
15. K. Sung, D. Haderski, A. Hiltner, and E. Baer, *J. Appl. Polym. Sci.,* **52,** 147 (1994).
16. K. Sung, A. Hiltner, and E. Baer, *J. Mater. Sci.,* **29,** 5559 (1994).
17. T. Kurauchi and T. Ohta, *J. Mat. Sci.,* **19,** 1699 (1984).
18. R. E. Robertson, *J. Adhes.,* **4,** 1 (1972).
19. H. R. Brown, *J. Mater. Sci.,* **25,** 2791 (1990).

20. C. Creton, E. J. Kramer, C.-Y. Hui, and H. R. Brown, *Macromolecules,* **25,** 3075 (1992).
21. S. Mostovoy and E. J. Ripling, *J. Appl. Polym. Sci.,* **15,** 661 (1971).
22. W. D. Bascom, R. L. Cottingtion, R. L. Jones, and P. Peyser, *J. Appl. Polym. Sci.,* **19,** 2545 (1975).
23. A. J. Kinloch and S. J. Shaw, *J. Adhes.,* **12,** 59 (1981).
24. D. A. Schupp and W. W. Gerberich, *J. Adhes.,* **35,** 269 (1991).
25. W. J. Schrenk, U.S. Pat. 3,884,606 (1975).
26. C. D. Mueller, S. Nazarenko, T. Ebeling, T. L. Schuman, A. Hiltner, and E. Baer, *Polym. Eng. Sci.,* **37,** 355 (1997).
27. R. A. Mendelson, in *Detection and Data Analysis in Size Exclusion Chromatography,* T. Provder, Ed., American Chemical Society, Washington, DC, 1987, pp. 263–280.
28. T. Ebeling, A. Hiltner, and E. Baer, in *Interfacial Aspects of Multicomponent Materials,* D. J. Lohse, T. P. Russell, and L. H. Sperling, Eds., Plenum, New York, 1997, pp. 95–106.
29. M. J. Guest and J. H. Daly, *Eur. Polym. J.,* **25,** 985 (1989).
30. T. A. Callaghan, K. Tokakawa, D. R. Paul, and A. R. Padwa, *Polymer,* **34,** 3796 (1993).
31. K. Kendall, *J. Adhes.,* **5,** 105 (1973).
32. D. Haderski, K. Sung, J. Im, A. Hiltner, and E. Baer, *J. Appl. Polym. Sci.,* **52,** 121 (1994).
33. A. J. Hsieh, N. S. Schneider, and J. F. Mandell, *Polym. Compos.,* **4,** 240 (1990).
34. J. R. Rice, *J. Appl. Mech.,* **55,** 99 (1988).
35. A. K. Gautesen and J. Dundurs, *J. Appl. Mech.,* **54,** 93 (1987).
36. H. R. Brown, *Macromolecules,* **24,** 2752 (1991).
37. H. R. Brown, *J. Mater. Sci.,* **25,** 2791 (1990).
38. S. S. Wang, J. F. Mandell, and F. J. McGarry, *Int. J. Fract.,* **14,** 39 (1978).
39. D. H. Kaeble, *J. Adhes.,* **37,** 205 (1992).